ELSEVIER

Earth and Planetary Science Letters 183 (2000) 245–259

EPSL

www.elsevier.com/locate/epsl

Boomerang Seamount: the active expression of the Amsterdam–St. Paul hotspot, Southeast Indian Ridge

K.T.M. Johnson [a,*], D.W. Graham [b], K.H. Rubin [c], K. Nicolaysen [d], D.S. Scheirer [e], D.W. Forsyth [e], E.T. Baker [f], L.M. Douglas-Priebe [b]

[a] *Department of Geology, Bishop Museum, Honolulu, HI 96817, USA*
[b] *College of Oceanic and Atmospheric Sciences, Oregon State University, Corvallis, OR 97331, USA*
[c] *Department of Geology and Geophysics, University of Hawaii, Honolulu, HI 96822, USA*
[d] *Department of Earth, Atmospheric, and Planetary Sciences, Massachusetts Institute of Technology, Cambridge, MA 02139, USA*
[e] *Department of Geological Sciences, Brown University, Providence, RI 02912, USA*
[f] *Pacific Marine Environmental Laboratory, National Oceanic and Atmospheric Administration, Seattle, WA 98115, USA*

Received 15 September 1999; received in revised form 18 August 2000; accepted 19 September 2000

Abstract

During a survey of the axis of the Southeast Indian Ridge (SEIR), we discovered a 1100 m tall, volcanically active submarine volcano, Boomerang Seamount, near the spreading center on the Amsterdam–St. Paul (ASP) Plateau. The summit of the volcano is 650 m below sea level and has a 200-m-deep, 2-km-wide circular caldera. Samples of very fresh volcanic glass, dated by the ^{210}Po–^{210}Pb technique at $\sim$5 months old, were collected from the floor of the caldera in March 1996. The volcano is 18 km northeast of Amsterdam Island near the intersection of a long spreading segment and the Boomerang Transform Fault. It is built on the stationary Antarctic Plate, where widely scattered volcanic activity thickens the crust, continuing to build the plateau. Water column profiles reveal a 1.7°C temperature anomaly and a 0.3 V stepped nephelometer (water column turbidity) anomaly within the caldera, nearly an order of magnitude larger than other hydrothermal plume anomalies we measured. These anomalies suggest hydrothermal activity within the caldera. Volcanic glass compositions at two sample sites on the volcano summit are similar to each other and to Amsterdam and St. Paul Island basalts, but have some important differences as well. K_2O/TiO_2 ratios in Boomerang Seamount glasses are similar to St. Paul Island samples, but differ significantly from Amsterdam Island samples. Rare earth element patterns in lavas from Boomerang, Amsterdam, and St. Paul are similar. Sr, Nd, and Pb isotope ratios in samples from the Boomerang Caldera floor are similar to samples from Amsterdam Island. However, another sample from Boomerang Seamount deviates from a SEIR–St. Paul–Amsterdam mixing trend and shows evidence of mixing with a Kerguelen-like source component. The geochemical complexity of these three closely spaced volcanic edifices on the ASP Plateau suggests that the Boomerang Seamount source is heterogeneous on a very small scale.

Keywords: mantle plumes; hot spots; Southeast Indian Ridge; hydrothermal conditions; Amsterdam Island; Saint Paul Island

* Corresponding author. Tel.: +1-808-848-4124; Fax: +1-808-847-8252; E-mail: kevinj@soest.hawaii.edu

0012-821X/00/$ – see front matter
PII: S0012-821X(00)00279-X

1. Introduction

The Amsterdam–St. Paul (ASP) Plateau is an oceanic platform that rises 1000–1500 m above the adjacent seafloor and sits atop the Southeast Indian Ridge (SEIR) (Fig. 1). The SEIR itself extends 6000 km from the Rodrigues Triple Junction to the Macquarie Triple Junction and is one of three major spreading centers in the Indian Ocean. Volcanic construction on the ASP Plateau is widespread; it occurs at the SEIR spreading center, in some diffuse off-axis areas, and at edifices such as Amsterdam and St. Paul Islands [1]. A 53-day expedition to this region in February–April 1996 on the R/V *Melville* (Boomerang Expedition, Leg 6) mapped some 1400 km of the SEIR with 75–100% Seabeam coverage and sampled along the spreading center at an average dredge and core spacing of 14 km on either side of the ASP Plateau, and 10 km on the ASP Plateau [2,3].

During the course of the survey, we discovered an 1100-m-high seamount rising to a depth of 650 m below sea level 18 km northeast of Amsterdam Island and 120 km north of St. Paul Island (Fig. 1b). The seamount is surmounted by a circular summit caldera 2 km in diameter and 200 m deep. The summit region is highly reflective to side-scan sonar, indicating small-scale roughness of the seafloor that is characteristic of young, unsedimented lava flows [1]. Extremely fresh basalt glass was recovered from two sites on the seamount summit. The seamount appears to have at least two 40-km-long rift zones extending north and southeast from its summit, giving it an arcuate shape in plan view. For this reason, and because of the expedition's designation, the feature was named Boomerang Seamount. In this paper, we describe the morphological, geochemical, and hydrothermal characteristics of Boomerang Seamount and discuss it in the context of mantle plume activity in the region.

2. Geologic setting

Australia and Antarctica began to separate around 110 Myr, but seafloor spreading along what has become the SEIR began during the Eocene. This caused the Kerguelen Plateau and Broken Ridge to separate at the site of the Kerguelen hotspot, now located ~1400 km southwest of the

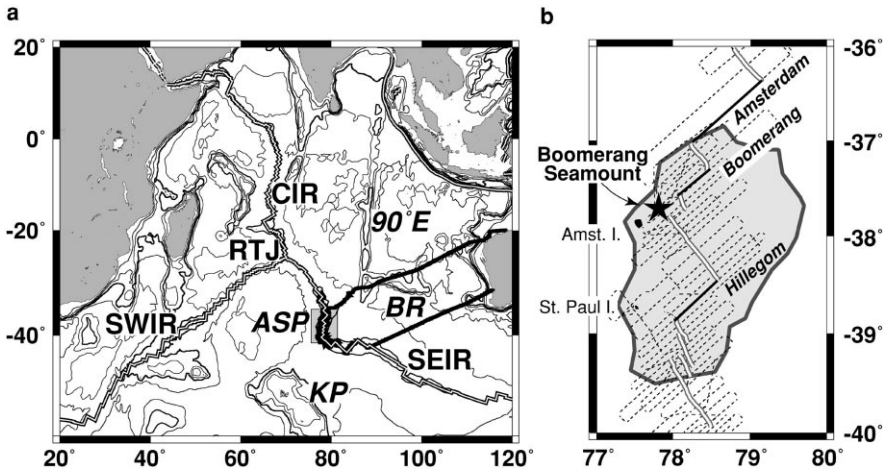

Fig. 1. (a) The Indian Ocean, its three main spreading centers (double lines), and selected hotspot features. Contour interval is 1 km. Thick line is the Boomerang Leg 6 cruise track and the shaded box is coverage area of (b). 90°E – Ninetyeast Ridge; ASP – Amsterdam–St. Paul Plateau; BR – Broken Ridge; KP – Kerguelen Plateau; SWIR – Southwest Indian Ridge; RTJ – 16 Rodrigues Triple Junction; CIR – Central Indian Ridge; SEIR – Southeast Indian Ridge. (b) Blow-up of the ASP Plateau showing 2000 m depth contour used to define the Plateau (dark gray), track line (dashed line), mapped ridge segments (double lines), fracture zones (heavy lines with italicized names), and the locations of Amsterdam and St. Paul Islands and Boomerang Seamount (star).

ASP 2 Plateau (Fig. 1) [4–7]. Since then, the SEIR has been migrating to the northeast away from the hotspot and currently spreads at a full-rate of ~65 mm/yr. Because the Antarctic Plate is essentially fixed in the hotspot reference frame [8], the Australian Plate migrates over the deep mantle at the total opening rate of the SEIR and the ridge migrates northeastward at approximately half that rate (32–33 mm/yr). The ASP hotspot was originally located beneath the Australian Plate, and it may have contributed to the formation of Ninetyeast Ridge until separation of Broken Ridge and Ninetyeast Ridge from the Kerguelen Plateau at about 40 Ma [9–11]. Satellite altimetry [12] shows a chain of seamounts connecting the southern tip of the Ninetyeast Ridge to the northern edge of the ASP Plateau. This seamount chain appears to delineate the ASP hotspot track on the Australian Plate subsequent to the breakup of the Kerguelen Plateau and Broken Ridge. Since the SEIR passed over the ASP hotspot 3–5 million years ago [13], the hotspot currently lies beneath the nearly stationary Antarctic Plate southwest of the SEIR. Its stationary location has allowed the formation of the shallowest parts of the ASP Plateau through continued activity at island and seamount volcanoes.

3. Results

3.1. Seamount morphology

The currently most active surface expression of the ASP hotspot may be the Boomerang Seamount. The Boomerang Seamount lies nearly at the intersection of a long, straight spreading segment that bisects the ASP Plateau and a transform fault near the northwest edge of the plateau (Fig. 2a). This ridge segment (I2) shows high $^3He/^4He$ ratios (>9 R_A), a diagnostic characteristic of the ASP hotspot [3]. The southern section of segment I2 (I2S) appears to terminate just to the southeast of the seamount, sidestepping the summit through a short, 10-km-long spreading segment on the northeast flank of the seamount (I2N) that links to the Boomerang Transform Fault (Fig. 2a). The southeast rift zone of Boomerang Seamount is parallel to the trend of segment I2S and its orientation may be controlled by either the pre-existing structure developed at the spreading axis or by the regional stress field controlling the orientation of the ridge axis.

Within the arc formed by the two main north and southeast rift zones is another shallow edifice, smaller than the main edifice, that possesses a short NNE-trending ridge of its own. This smaller edifice is located at the projected intersection of segment I2S and the Boomerang Transform Fault. The base of Boomerang Seamount occurs over a range of depths from 1600 m to 2000 m, thereby giving the seamount a range of base to summit heights from 950 m to 1350 m; for simplicity in this paper, we have chosen 1100 m as an average height of the seamount. Using these parameters, the volume of Boomerang Seamount is calculated to be ~300 km^3, which when combined with the approximate age of the seafloor on which it sits of 700 000 yr yields a minimum growth rate of ~0.0004 km^3/yr, or about 1.5 orders of magnitude smaller than the growth rate for Mauna Loa volcano in Hawaii.

The surfaces of the volcanic edifices are relatively smooth, with evidence for small satellite cones away from the summit area and lobe-shaped topographic plateaus and terraces downslope of the ridge axes (Fig. 2a). The summit of Boomerang Seamount contains a 2-km-wide caldera with a nearly constant 200 m depth and a volume of ~0.63 km^3. Within the SW section of the caldera, several smaller, nested collapse features can be seen. Small, discontinuous ring fault scarps can be clearly seen 1–2 km west of the caldera (Fig. 2b). They may also be present in the southeast sector of the summit where the multibeam bathymetry data are less clear or incomplete. The steep slopes of the caldera walls, generally greater than 45°, suggest an origin by faulting and subsequent mass-wasting rather than by explosive excavation or by build-up of basaltic lava flows along ring fractures. Likewise, the near-circularity of the walls and their nearly constant height suggest formation of the caldera by down-drop of the center along a continuous ring fault system, the upper reaches of which now form the caldera walls.

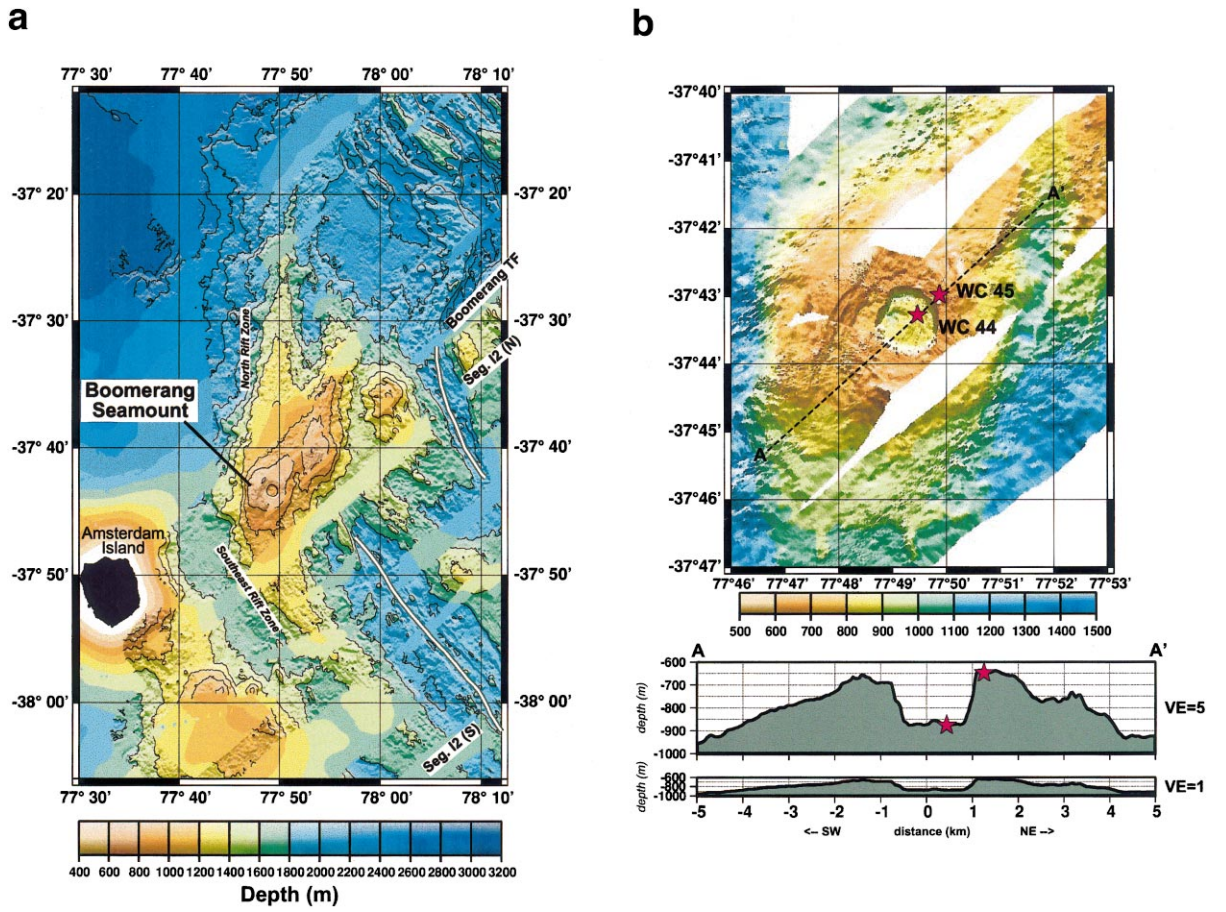

Fig. 2. (a) Bathymetry of Boomerang Seamount region. Areas that are contoured at 200 m intervals are covered by Seabeam 2000 data. Other areas are interpolated or controlled by other shipboard bathymetric measurements or satellite gravity data. Thick white lines represent ridge segments. (b) Top panel is Seabeam 2000 bathymetry (ping data) illuminated from the north, with wax core stations 44 and 45 plotted as blue stars. Bottom panels are bathymetric cross-sections of the caldera along section A–A′ in the top panel, plotted at five times and one time vertical exaggerations.

3.2. Geochemistry

3.2.1. Basaltic glass

Volcanic glass samples were collected from the floor of the summit caldera (wax core sample WC44) and from just outside the caldera rim (WC45) (Fig. 2). Samples were collected using a single-head wax coring device with a wax head diameter of approximately 30 cm and a weight of approximately 315 kg. At these two sites, a double hit technique was used to improve sample recovery: after the initial impact at 90 m/min lowering rate, the device was raised to 100 m above the seafloor, allowed to steady in the water column, and lowered again at 90 m/min for a second impact. Although these cores were not located by transponders, experience with transponder-navigated wax cores elsewhere suggests that the area of seafloor sampled using this double hit technique is approximately 8–10 m in diameter. Sample recovery in WC44 was ~50 g of glass and in WC45 ~250 g of glass and ~150 g of red mud.

Rock compositions were determined on glass chips recovered from the wax core. The glass samples are highly vesicular, very fresh and appear to be quite young. Preliminary chemical groups were

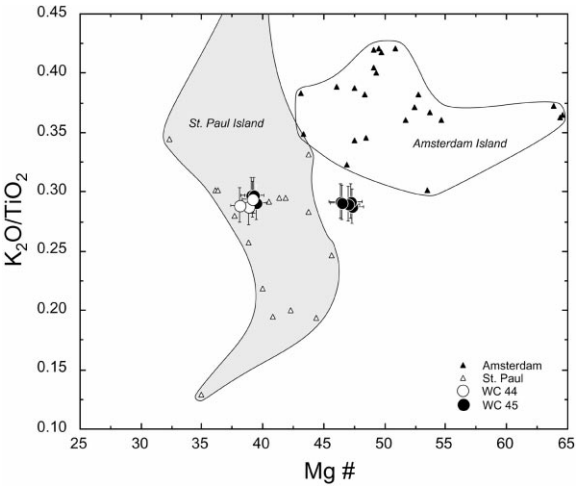

Fig. 3. K_2O/TiO_2 versus Mg# (Mg/[Mg+Fe*]×100) for Boomerang Seamount samples and samples from Amsterdam and St. Paul Islands. Fields for basalts from the two islands are drawn around samples with $SiO_2 \leq 51\%$ for comparison with Boomerang Seamount data. The open triangles are data for dikes from the northeast-facing scarp on the southern side of the breached caldera on St. Paul (this study and [17,32]). The three small squares are hawaiites from St. Paul with $SiO_2 > 54\%$ [32,33,41]. The two chemical groups in WC45 and their relationship with WC44 and some St. Paul samples are shown. 2σ error bars are shown for the Boomerang Seamount samples. All Fe is calculated as Fe^{2+}. Data sources: [17,30–33,41]; F. Frey and D. Weis, unpublished data for Amsterdam Island; W. White, unpublished data for Amsterdam and St. Paul Islands.

determined on the basis of major element analyses of randomly selected glass chips from each core (WC44a–c and WC45a–h; Table 1) by electron microprobe. Each major element analysis in Table 1 represents the average of at least three probe points along a transect of a single chip of glass. Analyses with totals outside of 98–101% were excluded. On this basis, we identified one chemical group in WC44 and two groups in WC45. The glasses are tholeiitic to transitional in major element composition and are similar to some St. Paul Island lavas. The glasses differ significantly, however, from the more proximal lavas erupted at Amsterdam Island, for example in K/Ti at a given Mg# (Fig. 3). Moreover, there are significant compositional differences between the two chemical groups recovered in WC45 (Table 1 and Fig. 3), although these differences may result from shallow-level fractional crystallization of olivine and plagioclase ± clinopyroxene. The WC44 glasses are similar in major element composition to one of the groups in WC45, but are slightly more evolved. New analyses of glasses from two dikes on St. Paul Island are also reported in Table 1.

Rare earth element (REE) concentrations and patterns in WC44 and WC45 glasses are similar to those in basalts from St. Paul Island. The only two rocks from Amsterdam Island with REE analyses and two other rocks from St. Paul Island have positive Eu anomalies and appear to be plagioclase cumulates, so are not directly comparable to the glasses from Boomerang Seamount (Fig. 4a).

Isotopic compositions of $^{87}Sr/^{86}Sr$, $^{143}Nd/^{144}Nd$,

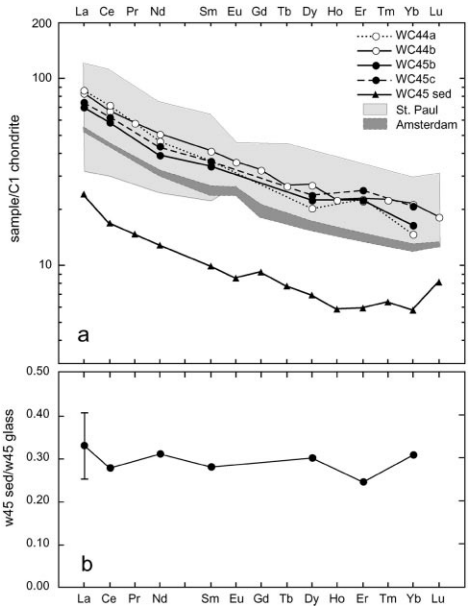

Fig. 4. (a) Chondrite-normalized REE plot of samples from Boomerang Seamount, Amsterdam and St. Paul Islands. Two St. Paul samples and the only two samples from Amsterdam Island have lower REE abundances and positive Eu anomalies suggestive of plagioclase accumulation. Data sources: [17,18,21]; F. Frey and D. Weis, unpublished data for Amsterdam Island; W. White, unpublished data for Amsterdam and St. Paul Islands. Chondrite normalization values of Anders and Grevesse [42]. (b) REE concentrations of the sediment recovered in WC45 normalized to the average of the two WC45 glass analyses. Note that the *y*-axis is linear. Propagated error bar is shown.

Table 1
Major and trace element composition of glasses from Boomerang Seamount and St. Paul Island

	Boomerang Seamount												St. Paul Island	
	WC44a[a]	WC44b	WC44c	WC45a	WC45b[a]	WC45c[a]	WC45d	WC45e	WC45f	WC45g	WC45h	WC45sed	SP-1a[a]	SP-5b[a]
Lat (°S)	37.721	37.721	37.721	37.716	37.716	37.716	37.716	37.716	37.716	37.716	37.716	37.716	38.72	38.72
Long (°E)	77.825	77.825	77.825	77.832	77.832	77.832	77.832	77.832	77.832	77.832	77.832	77.832	77.55	77.55
Depth (m)	875	875	875	647	647	647	647	647	647	647	647	647		
SiO_2	50.73	50.98	51.07	50.76	50.80	50.99	50.98	50.86	50.35	50.55	50.39		50.63	50.29
TiO_2	2.63	2.69	2.60	2.12	2.11	2.53	2.14	2.55	2.13	2.54	2.16		3.29	3.23
Al_2O_3	13.54	13.50	13.60	14.26	14.09	13.78	14.25	13.66	14.07	13.67	13.99	0.48	13.37	13.33
FeO*	13.11	13.30	13.07	11.67	11.60	13.09	11.98	13.36	11.95	13.23	11.84	49.24	14.18	13.92
MnO	0.22	0.20	0.24	0.21	0.21	0.22	0.18	0.18	0.19	0.22	0.20	0.049	0.24	0.22
MgO	4.66	4.59	4.71	5.88	5.81	4.79	5.96	4.78	5.80	4.80	5.78	0.72	4.49	4.45
CaO	9.29	9.22	9.36	10.52	10.50	9.28	10.66	9.43	10.56	9.28	10.56	1.11	8.91	8.78
Na_2O	3.09	3.00	3.06	2.80	2.82	3.02	2.93	3.19	2.83	3.19	2.90		3.25	3.14
K_2O	0.75	0.78	0.76	0.61	0.62	0.74	0.62	0.76	0.62	0.75	0.63		0.99	0.97
P_2O_5	0.31	0.31	0.30	0.25	0.22	0.30	0.28	0.30	0.23	0.30	0.26	0.42	0.41	0.45
Total	98.33	98.58	98.78	99.10	98.79	98.75	100.00	99.09	98.76	98.56	98.71		99.76	98.77
Mg/(Mg+Fe*)	0.3879	0.3809	0.3911	0.4730	0.4718	0.3949	0.4703	0.3897	0.4639	0.3929	0.4655		0.3606	0.3631
K_2O/TiO_2	0.287	0.289	0.294	0.288	0.292	0.291	0.290	0.297	0.292	0.297	0.291		0.301	0.301
Ti												23.4		
V		386										105		
Cr		17										12		
Co		41										8.5		
Ni		22										7.6		
Cu		57										136		
Zn		118										481		
As		1.8										44		
Rb		15.7										2.9		
Sr		264										206		
Y		33										9.0		
Zr		175										33		
Nb		28										4.9		
Mo		1.03										13		
Cs		0.198										0.067		
Ba		205										71		
La	20.4	19.8			16.6	17.6						5.7	21.2	20.4
Ce	44.4	41.5			36.0	38.7						10.4	48.6	46.6
Pr		5.2										1.3		
Nd	21.3	23.4			18.0	20.2						6.0	24.7	24.0
Sm	5.1	5.8			4.8	5.2						1.4	6.5	5.6
Eu		1.9										0.46	3.2	2.9

Table 1 (*continued*)
Major and trace element composition of glasses from Boomerang Seamount and St. Paul Island

	Boomerang Seamount												St. Paul Island	
	WC44a[a]	WC44b	WC44c	WC45a	WC45b[a]	WC45c[a]	WC45d	WC45e	WC45f	WC45g	WC45h	WC45sed	SP-1a[a]	SP-5b[a]
Gd		6.4										1.8		
Tb		0.94										0.27		
Dy	4.9	6.5			5.4	5.7						1.7	6.6	5.9
Ho		1.2										0.32		
Er	3.5	3.6			3.6	4.1						0.94	4.2	4.0
Tm		0.49										0.14		
Yb	2.4	3.5			2.7	3.4						1.0	4.2	4.0
Lu		0.44										0.20		
Hf		4.9										1.1		
Ta		1.9										0.36		
Pb		1.537			0.224							26.3	1.89	
Th		2.372												
U		0.591												
$^{87}Sr/^{86}Sr$		0.70381			0.70456								0.70360	
$^{143}Nd/^{144}Nd$		0.51284			0.51279								0.51289	
$^{206}Pb/^{204}Pb$		19.139			18.554								18.651	
$^{207}Pb/^{204}Pb$		15.618			15.586								15.558	
$^{208}Pb/^{204}Pb$		39.472			39.036								38.842	

Major elements were analyzed by electron microprobe at Oregon State University (L. Douglas-Priebe, analyst). Precision is $<1\%$ for major elements and 5–7% for K and P. Mg/(Mg+Fe*) assumes all Fe is Fe^{2+}. Major elements in WC45sed by ICP-AES at Oregon State University are elemental wt%. Trace elements were analyzed by ICP-MS at University of Hawaii, except Th and U concentrations, which were analyzed by TIMS on the UH Sector54 following anion exchange extraction from dissolved glass chips [14]. Precision, based on replicate analysis of reference standards, is 1–3% for REE and 2–25% for other ICP-MS trace elements. Th and U procedural blanks are <2 pg and external reproducibilities are better than 0.2%. Data are reported relative to a value of $^{143}Nd/^{144}Nd = 0.511850$ for the La Jolla Nd standard, and $^{87}Sr/^{86}Sr = 0.71025$ for NBS ^{987}Sr. Isotopic fractionation corrections are $^{148}NdO/^{144}NdO = 0.242436$ ($^{148}Nd/^{144}Nd = 0.241572$); Pb isotope ratios are corrected for fractionation using the NBS 981 standard values of Todt et al. [15]. Within-run errors on the isotopic data above are less than or equal to the external uncertainties on these standards: the total range measured (last 2 yr) for NBS 987 Sr is

[a]REE in these samples were analyzed by ion microprobe at Woods Hole Oceanographic Institution. Accuracy ± 5–10%; precision ± 1–8%.

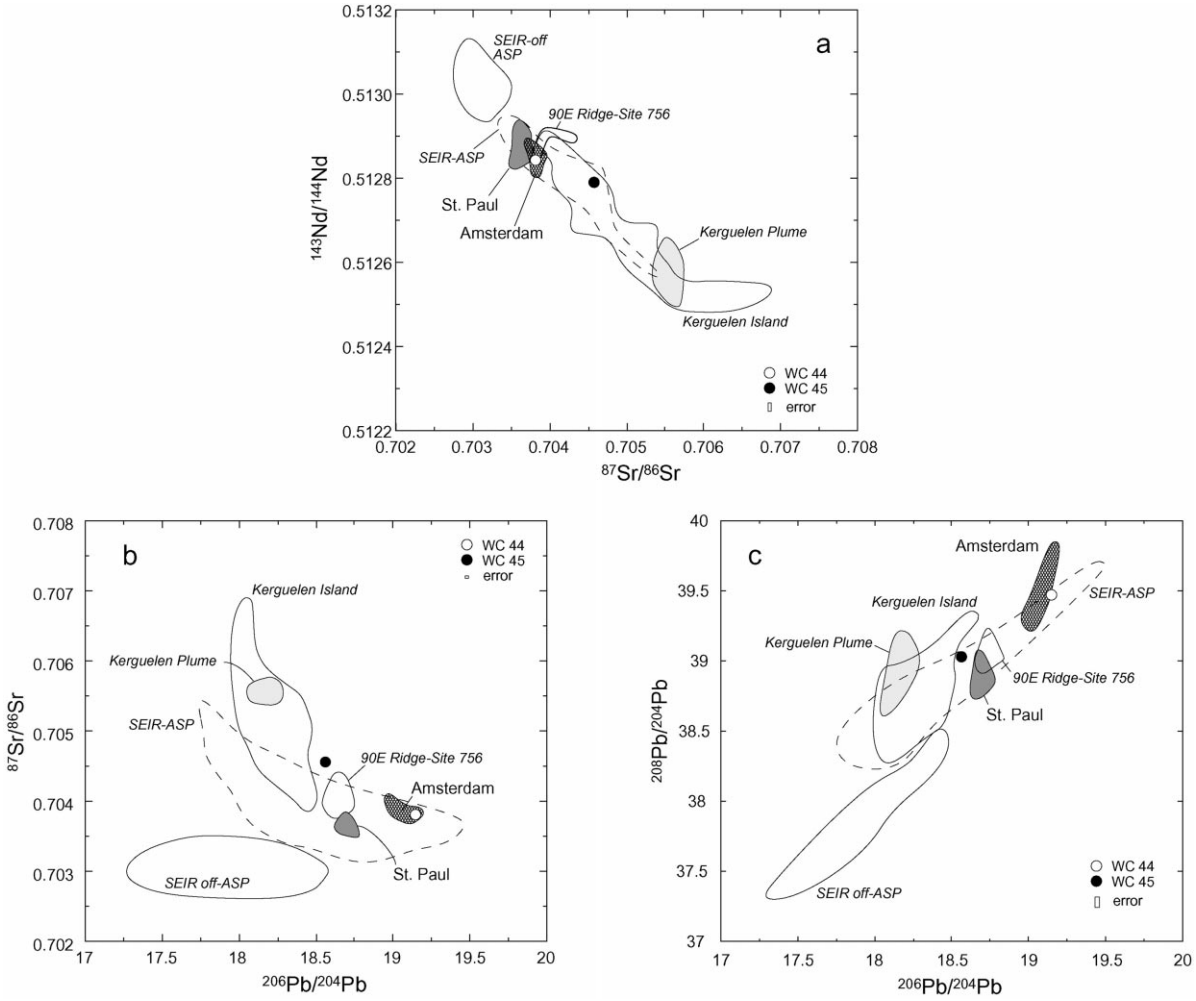

Fig. 5. Isotope compositions of Boomerang glasses and whole rock and glass samples from Amsterdam and St. Paul Islands ([17–21]; F. Frey and D. Weis, unpublished data; W. White, unpublished data). Amsterdam and St. Paul Islands are distinct on all plots. WC44 plots close to Amsterdam samples, while WC45 has less radiogenic Pb and Nd but more radiogenic Sr and plots away from WC44 and the islands. WC45 also plots either in the Kerguelen field or between the other data and the Kerguelen field. The 'SEIR–ASP' field encloses SEIR data from the ASP Plateau; 'SEIR–off ASP' field encloses all other available SEIR data. Field labeled 'Kerguelen Plume' described by Weis et al. [43]. Data sources for SEIR, Kerguelen and Ninetyeast Ridge: [17–22,43–49], K. Johnson, unpublished data. Error bars represent the total range of variation on analyses of isotope standards measured in the University of Hawaii lab over the last 2 yr.

$^{206}Pb/^{204}Pb$, $^{207}Pb/^{204}Pb$, and $^{208}Pb/^{204}Pb$ were determined on single chunks of glass from WC44 and WC45. There are important differences in isotopic compositions between Amsterdam and St. Paul Islands and between Boomerang Seamount and the islands. Amsterdam Island has higher $^{206}Pb/^{204}Pb$, $^{208}Pb/^{204}Pb$ and $^{87}Sr/^{86}Sr$ than St. Paul Island (Fig. 5; [17–21]; F. Frey and D. Weis, unpublished data; W. White, unpublished data). WC44 plots close to Amsterdam Island samples in all of the isotope plots. WC45 is higher in $^{87}Sr/^{86}Sr$ than Amsterdam and St. Paul samples, but lower in $^{206}Pb/^{204}Pb$ and $^{143}Nd/^{144}Nd$ (Fig. 5). Amsterdam, St. Paul, and WC44 plot in or close to the field for ODP site 756, drilled on the southern terminus of the Ninetyeast Ridge

[22], in Nd–Sr space (Fig. 5a), but only St. Paul and WC45 plot in or close to this field in Sr–Pb and Pb–Pb space (Fig. 5b,c). WC45 consistently plots between WC44, Amsterdam, and St. Paul and the field for Kerguelen Island (Fig. 5a–c).

3.2.2. ^{210}Po–^{210}Pb dating

A single chip of glass from WC44 was dated using the ^{210}Po–^{210}Pb technique [23] and was found to have an eruption window of 1 November 1995 to 29 December 1995. Po degasses from a lava upon eruption; due to uncertainty in the extent of initial Po degassing, we report ages using an 'eruption window' (the calendar dates correspond to maximum (100%) and minimum (75%) Po degassing based upon observed 100% and $>75\%$ Po degassing during the 40-m-deep 1989 eruption of Macdonald seamount [24] and the 1991–1992 eruption of 9–10°N EPR [23], respectively). A major control on Po degassing is likely hydrostatic pressure; because of the shallowness of this eruption, we feel the maximum age best approximates the actual age. Ages are calculated by regressing a time series of ^{210}Po measurements to the radioactive ingrowth curve. Typically at least three ^{210}Po analyses are used but only two analyses were possible for WC44. Nevertheless, it is safe to conclude that the sample was on the order of 5 ± 2 months old when collected on 30 March 1996.

3.2.3. Sediment

WC45 from the rim of the summit caldera recovered 250 g of glass and rock fragments with abundant red–brown sediment. The major element and chalcophile trace element composition of this sediment (Table 1) is grossly similar to high-Fe, low-Mn ochres and ferruginous umbers from Cyprus and the TAG area of the Mid-Atlantic Ridge [25–27], although the WC45 sediment is higher in Fe (49.24 elemental wt%) and lower in Mn (491 ppm) than the ochres and umbers from either location. While the Fe/Mn ratio in WC45 sediment is $\sim$two times higher ($\sim$1000) than that in Cyprus umbers and ochres (1–556), Ba/Cr, Sr/Cr, Cu/Zr, and Co/Ni in the WC45 sediment are within the ranges reported for Cyprus [26]. Pb concentration in WC45 sediment (26 ppm) is also similar to Pb values in Cyprus samples (12–219) [26].

Chondrite-normalized REE patterns from the WC45 sediment are parallel to WC44 and WC45 glass patterns, but are lower in REE concentration than the glasses (Fig. 4a). Normalizing WC45 sediment to WC45 glass produces a relatively flat pattern at about 0.3 times the glass concentration (Fig. 4b).

3.3. Water column

Portable, wire-mounted instruments called Miniature Autonomous Plume Recorders (MAPRs) designed to measure water column physical properties were used at all dredge and wax core sites [28]. The purpose of the MAPR is to provide rapid detection of hydrothermal activity during near-bottom operations where water column information would otherwise not be obtained, thereby using valuable ship time more efficiently. The instrument contains a nephelometer to measure the backscatter intensity of the water (related to particulate matter in the water), and

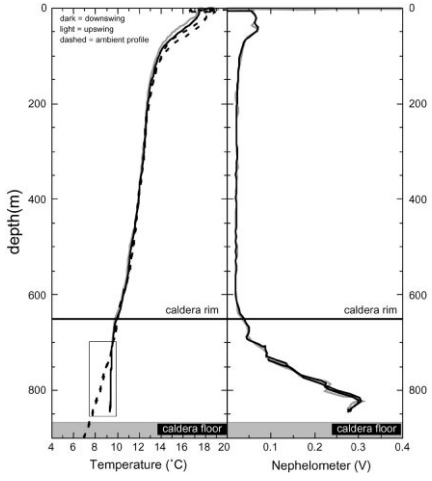

Fig. 6. MAPR temperature and nephelometer profiles collected from the WC44 deployment. Dark lines are data collected on the downswing and lighter lines are from the upswing. The dashed line marked 'ambient profile' is from the nearest deeper-water temperature profile to Boomerang Seamount. The nephelometer profiles are a three-point moving median filter that clearly shows the layered nature of the anomaly within the caldera (see text). The box around the lower portion of the temperature profile draws attention to the 1.6–1.7°C temperature anomaly discussed in the text.

temperature and pressure sensors. It was attached to the hydro-wire 30 m above the wax core and records data during both lowering and raising of the wire [29].

The MAPR profile collected from the center of the summit caldera is shown in Fig. 6. Within 100 m of the caldera floor, the nephelometer anomaly is 0.3 V, nearly an order of magnitude larger than plume anomalies we measured elsewhere on the SEIR [28]. Inflections in the nephelometer profile suggest stratification in several distinct water layers from the base of the caldera to its rim (Fig. 6).

The temperature profiles of nearby MAPR lowerings are nearly identical in the 400–1000 m depth range, and they parallel that of the deployment into the summit caldera at depths shallower than 650 m. Below that depth, the caldera temperatures are 1.6–1.7°C warmer than temperatures both extrapolated from the gradient above the summit caldera and associated with similar water depths outside the caldera (Fig. 6).

4. Discussion

The discovery of an volcanically active seamount in a poorly studied region of the Indian Ocean is a significant finding. First, active volcanism on the ASP Plateau was poorly documented prior to this survey, and the history of subaerial volcanism at the two islands still remains poorly understood [30–33]. Second, the current chemical composition and geographic location of active ASP hotspot magmatism is important in understanding plume–ridge interaction and in evaluating the submarine eruptive history of the ASP hotspot. Third, the discovery of the volcanically active Boomerang Seamount provides an opportunity to study the effects of volcanism at a shallow submarine caldera upon the dispersal of hydrothermal effluent, the formation of submarine mineral deposits, and the origin of biological niches in the Indian Ocean.

4.1. Active hotspot volcanism

Off-axis volcanism on the ASP Plateau is widely scattered rather than concentrated at a single eruptive center [1,2]. Both Amsterdam Island and St. Paul Island have had historical volcanic activity [33]; the last Amsterdam eruption was more than 100 yr ago and the most recent volcanic eruption on St. Paul was in 1793. We observed several active fumaroles along the inner walls of the St. Paul caldera during a brief visit in 1996. Boomerang Seamount has clearly had the most recent eruption of these three volcanic edifices.

The basalt glasses from the two sites at Boomerang Seamount are similar to, but have some important differences from, volcanic rocks at both Amsterdam and St. Paul Islands in major and trace elements and isotopes. Moreover, there appear to be significant major element and isotopic differences between WC44 and WC45, as well as major element differences within WC45 itself.

The grouping of the data within Mg#–K_2O/TiO_2 space illustrates the differences between Amsterdam, St. Paul, and the Boomerang samples (Fig. 3). First, samples from Amsterdam and St. Paul Islands generally plot in distinct fields, although one St. Paul sample plots within analytical uncertainty of the Amsterdam field. Boomerang Seamount and Amsterdam Island, although separated by only 18 km, are also different in K_2O/TiO_2 with Amsterdam Island being generally more enriched at a given Mg#. St. Paul Island lavas show much more compositional diversity than Amsterdam lavas, but a cluster of samples, from chilled dike margins on the northeast-facing scarp of the southern side of the breached caldera on St. Paul (this study and [17,32]), are compositionally similar to some of the Boomerang Seamount samples (triangles in Fig. 3).

The major element differences between WC44 and WC45, and between the two compositional groups in WC45 may be largely explained by crustal-level fractional crystallization of olivine, clinopyroxene, and plagioclase. However, the Sr, Nd, and Pb isotope compositions discussed below require that different parental magmas are involved. These different parental magmas must have been produced by partial melting of an isotopically heterogeneous mantle source.

The close similarity between Boomerang Sea-

mount and St. Paul lavas shown in Fig. 3 does not extend to Sr–Nd–Pb isotope compositions. Plots of $^{87}Sr/^{86}Sr$, $^{143}Nd/^{144}Nd$, and $^{206}Pb/^{204}Pb$ (Fig. 5) show that, in general, lavas from Amsterdam and St. Paul Islands are isotopically distinct, although there is some overlap in $^{87}Sr/^{86}Sr$ vs. $^{143}Nd/^{144}Nd$ (Fig. 5a). In plots of $^{206}Pb/^{204}Pb$ vs. $^{87}Sr/^{86}Sr$ and $^{208}Pb/^{204}Pb$, Boomerang samples plot outside of the field for St. Paul lavas, but WC44 plots within the field for Amsterdam lavas (Fig. 5b,c). Although the Boomerang, Amsterdam, and St. Paul samples all plot in or near the field for other SEIR lavas from the ASP Plateau, only WC45 consistently plots near the field for Kerguelen lavas, and it appears to deviate from any trajectory that might be defined by WC44, Amsterdam, St. Paul, and off-plateau SEIR lavas.

We infer that the mantle underlying the Boomerang Seamount area is isotopically heterogeneous on a very small scale and that blobs of mantle with a Kerguelen Island isotopic signature are contained in the melting regime for Boomerang Seamount. The isotope data indicate that the mantle source for the three volcanic centers probably contains different proportions of at least three components. These components include a radiogenic Pb component, best characterized by the WC44 and Amsterdam Island lavas; a depleted mantle component, exemplified by MORB sampled along the SEIR away from the plateau; and an enriched component that is akin to the Kerguelen hotspot, and best represented at Boomerang Seamount by WC45. The scale of mantle source heterogeneities must be very small, probably on the order of 1 km, in order to account for these measurable isotopic differences at Boomerang Seamount.

Collectively, Boomerang Seamount, Amsterdam, and St. Paul Island lavas generally overlap the Sr–Nd–Pb isotope compositions seen for Ninetyeast Ridge, in particular ODP site 756 on the southern terminus of the Ninetyeast Ridge (Fig. 5). This is significant given the tectonic reconstruction, wherein the Ninetyeast Ridge may have been built in part by the ASP hotspot [9,21,22]. A line of submarine volcanoes northeast of the ASP Plateau appears to be the trace of the ASP hotspot. This trace would have formed on the Australian Plate between the time that the Kerguelen Plateau split from Broken Ridge and Ninetyeast Ridge and the time that the ASP plume hotspot was 'captured' by the approaching SEIR. It appears that the ASP hotspot stopped forming this chain on the Australian Plate between 5 and 10 Ma when hotspot volcanism was intercepted by the SEIR, which had been migrating towards it [1]. Once captured by the ridge, the hotspot was able to build up a shallow platform by adding to the volcanic accretion at the spreading center. Currently, the locus of ASP hotspot volcanism appears to be wholly on the Antarctic Plate, where it has formed the islands and Boomerang Seamount, among other constructive features. Thus, the observed isotopic similarities between Boomerang Seamount, the islands, and Ninetyeast Ridge are consistent with the genesis of these features from the same hotspot at different stages of its evolution. This is also consistent with the assertion that the Ninetyeast Ridge was formed by a combination of two plume sources, one of which is similar to that which formed St. Paul Island [21].

4.2. Sediment

The red–brown sediment recovered in WC45 has both hydrothermal and non-hydrothermal characteristics. Its major and chalcophile trace elements are similar to hydrothermally derived ochres in both Cyprus [25,26] and the Mid-Atlantic Ridge at TAG [34], suggesting it was formed in a similar environment and by a similar mechanism to those deposits. In particular, Ba/Cr, Sr/Cr, Cu/Zr, and Co/Ni and Pb in the WC45 sediment are within the ranges noted for Cyprus ochres and low-Mn umbers [26]. These types of deposits are thought to form by oxidation of sulfide by a low temperature hydrothermal fluid, combined with precipitation of Fe oxide and silica from this fluid [35]. The non-hydrothermal character of the sediment is suggested by Fig. 4. The REE patterns for the sediment and the associated glass are parallel and unfractionated relative to each other, demonstrating a 'rock-like' REE profile for the sediment. Thus, it is possible that the

sediment comprises rock particles, carrying the REE signature of the glass, and hydrothermally derived Fe- and chalcophile-rich phases that dilute the total REE concentrations but do not change the REE signature.

It is also possible that the elevated chalcophile and metalloid concentrations we observe in sediments of Boomerang Caldera are related to degassing during the recent eruption itself. Rubin [36] proposed a basalt degassing explanation (i.e. the same way Po is lost from basalts, which allows us to date them) for very similar enrichments of Cu, Zn, Pb, and As (as well even larger enrichments in Mo, Sb, Sn and Pb) in particles from hydrocasts into the Loihi seamount pit crater that formed following the 1996 eruption. These Loihi particles also had indistinguishable Pb and Nd isotopic compositions from Loihi basalts, but slightly shifted Sr isotopic composition. The geochemical patterns of enrichment at Loihi could be predicted from a combination of relative element volatility during magmatic processes on land and solubility of these elements in seawater. The same process may have occurred at Boomerang resulting in the observed compositions of muds.

4.3. Water column

The MAPR profile (Fig. 6) collected from the center of the Boomerang Caldera suggests hydrothermal activity in the caldera. The 1.7°C temperature anomaly and the 0.3 V nephelometer anomaly are nearly an order of magnitude larger than the other plume anomalies we measured. At deep-sea hydrothermal sites elsewhere, such large optical backscatter anomalies have only been observed in the presence of volatile-rich fluids and/or relatively soon after an eruptive event which initiates or reinvigorates a hydrothermal system [37]. Although the precise source of the enhanced backscatter has not yet been identified, Baker et al. [37] suggest that elemental sulfur or biologically produced particles may efficiently scatter light of the $\sim$1 μm wavelength of the MAPR nephelometer.

The stratified nephelometer profile suggests layering of distinct water masses from the base of the caldera to its rim. A simple explanation of this stratification, seen on the up and down transits for each of the two impacts of WC44, is the influence of different chronic hydrothermal sources with different buoyancy fluxes. This hypothesis is supported by the presence of individual maxima and minima in the nephelometer profile (Fig. 6). An alternative hypothesis is stratification resulting from double-diffusive convection [38]. In either case, the stably stratified layers are preserved because the unbroken caldera rim creates an enclosed basin that prevents mixing with the surrounding water column. Water within the caldera originates as spill-over around the caldera rim, so its hydrographic properties reflect those at a depth of $\sim$650 m, modified by hydrothermal activity within the caldera. Staircase stratification of the water column is a phenomenon observed under hydrothermal conditions elsewhere. Layering of CO_2, density, temperature, conductivity, and pH in 100 and 200 m water column profiles were observed at Lakes Nyos and Monoun in Cameroon [39], and hot brine pools in deeps at the bottom of the Red Sea are stratified at depth scales of tens of meters [40].

5. Conclusions

A volcanically active submarine volcano, Boomerang Seamount, was discovered 18 km northeast of Amsterdam Island on the ASP Plateau near the SEIR. The seamount is in a region where the crust on the nearly stationary Antarctic Plate is being thickened by widespread volcanic activity. The 1100-m-high Boomerang Seamount is topped by a 2 km circular caldera in which extremely fresh, tholeiitic to transitional basalt glass was recovered. MAPR water column profiles within the caldera show evidence for hydrothermal activity as measured by large, stepped nephelometer anomalies.

Volcanic glass was recovered from two sampling sites, one from the caldera floor and the other along its rim. These glasses show chemical and isotopic similarities to lavas from Amsterdam and St. Paul Island, but they differ in detail. REE patterns in lavas from the three edifices are similar. K_2O/TiO_2 ratios are similar to some basalts

from St. Paul Island, but differ significantly from Amsterdam Island basalts. On the other hand, Sr, Nd, and Pb isotope ratios are similar in Amsterdam Island lavas and WC44 from the floor of Boomerang Seamount's summit caldera, but these differ significantly from St. Paul Island and WC45 compositions. Although there are significant differences between basalts from Boomerang Seamount and from the islands of Amsterdam and St. Paul, these basalts all display radiogenic $^{206}Pb/^{204}Pb$ ratios, and they are distinct from SEIR lavas erupted away from the ASP Plateau. Presence of Kerguelen-type source mantle beneath Boomerang Seamount is supported by the similarity of WC45 and Kerguelen isotope ratios. The consistent similarity of isotope compositions of Boomerang, Amsterdam, St. Paul, and youngest Ninetyeast Ridge lavas lends support to the idea that the ASP plume contributed to the formation of Ninetyeast, as suggested by others [9,21,22].

Acknowledgements

We thank Captain Eric Buck and the crew of the R/V *Melville* for their high level of professionalism during this long and sometimes difficult voyage. We are particularly grateful to Gene Pillard, Terry Naumann, and David Preston for their tireless handling of deck operations. Bill White, Fred Frey, and Dominique Weis kindly provided previously unpublished analyses of several Amsterdam and St. Paul Island samples. We thank Terres Australes et Antarctiques Françaises (TAAF) for their clearance to work in territorial waters around Amsterdam and St. Paul Islands. K.N. thanks J.J. Mahoney and K. Spencer for assistance with the Sr, Nd and Pb isotopic analyses. Constructive reviews by Rodey Batiza and Hubert Staudigel improved the manuscript. This work was supported by NSF-9415948, NSF-9505667, and the NOAA VENTS Program. This is PMEL contribution 2073.*[FA]*

References

[1] J.A. Conder, D.S. Scheirer, D.W. Forsyth, Seafloor spreading on the Amsterdam–St. Paul Plateau, J. Geophys. Res. 105 (B4) (2000) 8263–8277.

[2] D.S. Scheirer, D.W. Forsyth, J.A. Conder, M.A. Eberle, S.-H. Hung, K.T.M. Johnson, D.W. Graham, Anomalous seafloor spreading of the Southeast Indian Ridge near the Amsterdam–St. Paul Plateau, J. Geophys. Res. 105 (B4) (2000) 8243–8262.

[3] D.W. Graham, K.T.M. Johnson, L. Douglas-Priebe, J.E. Lupton, Hotspot-ridge interaction along the Southeast Indian Ridge near Amsterdam and St. Paul Islands: Helium isotope evidence, Earth Planet. Sci. Lett. 167 (1999) 297–310.

[4] J.C. Mutter, S.C. Cande, The early opening between Broken Ridge and Kerguelen Plateau, Earth Planet. Sci. Lett. 65 (1983) 369–376.

[5] A.A. Tikku, S.C. Cande, Early Tertiary reconstructions of the Australian and Antarctic plates, EOS Trans. Am. Geophys. Union 77 (1996) 689.

[6] S.C. Cande, J.C. Mutter, A revised identification of the oldest sea-floor spreading anomalies between Australia and Antarctica, Earth Planet. Sci. Lett. 58 (1982) 151–160.

[7] J.C. Mutter, K.A. Hegarty, S.C. Cande, J.K. Weissel, Breakup between Australia and Antarctica; a brief review in the light of new data, Tectonophysics 114 (1985) 255–279.

[8] A.E. Gripp, R.G. Gordon, Current plate velocities relative to the hotspots incorporating the NUVEL-1 global plate motion model, Geophys. Res. Lett. 17 (1990) 1109–1112.

[9] B.P. Luyendyk, W. Rennick, Tectonic history of aseismic ridges in the eastern Indian Ocean, Geol. Soc. Am. Bull. 88 (1977) 1347–1356.

[10] R.A. Duncan, M. Storey, The life cycle of Indian Ocean hotspots, in: R.A. Duncan, D.K. Rea, R.B. Kidd, U. von Rad, J.K. Weissel (Eds.), Synthesis of Results from Scientific Drilling in the Indian Ocean, Geophys. Monogr. 70, Am. Geophys. Union, Washington, DC, 1992, pp. 91–103.

[11] J.-Y. Royer, M.F. Coffin, Jurassic to Eocene plate reconstructions in the Kerguelen Plateau region, in: S.W. Wise, Jr., R. Schlich (Eds.), Proc. ODP, Sci. Results, 120, Ocean Drilling Program, College Station, TX, 1992, pp. 917–928.

[12] W.H. Smith, D.T. Sandwell, Measured and Estimated Seafloor Topography (version 4.2), World Data Center-A for Marine Geology and Geophysics, 1997.

[13] J.-Y. Royer, R. Schlich, Southeast Indian Ridge between the Rodriguez Triple Junction and the Amsterdam and Saint-Paul Islands: detailed kinematics for the past 20 m.y., J. Geophys. Res. 93 (1988) 13524–13550.

[14] K.H. Rubin, M.C. Smith, M.R. Perfit, L.F. Sacks, D. Christie, Geochronology and petrology of lavas from the 1996 North Gorda Ridge eruption, Deep-Sea Res. II 45 (1998) 2751–2799.

[15] W. Todt, R.A. Cliff, A. Hanser, A.W. Hofmann, Evaluation of a ^{202}Pb–^{205}Pb double spike for high-precision lead

isotopic analyses, in: A. Basu, S. Hart (Eds.), Earth Processes, Reading the Isotopic Code, 1996, pp. 429–437.
[16] J. Mahoney, C. Nicollet, C. Dupuy, Madagascar basalts: tracking oceanic and continental sources, Earth Planet. Sci. Lett. 104 (1991) 350–363.
[17] L. Dosso, H. Bougault, P. Beuzart, J.-Y. Calvez, J.-L. Joron, The geochemical structure of the South–East Indian Ridge, Earth Planet. Sci. Lett. 88 (1988) 47–59.
[18] A. Michard, R. Montigny, R. Schlich, Geochemistry of the mantle beneath the Rodriguez triple junction and the South–East Indian Ridge, Earth Planet. Sci. Lett. 78 (1986) 104–114.
[19] B. Hamelin, B. Dupré, C.-J. Allègre, Pb–Sr–Nd isotopic data of Indian Ocean ridges: new evidence of large-scale mapping of mantle heterogeneities, Earth Planet. Sci. Lett. 76 (1986) 288–298.
[20] B. Dupré, C.J. Allègre, Pb–Sr isotope variation in Indian Ocean basalts and mixing phenomena, Nature 303 (1983) 142–146.
[21] F.A. Frey, D. Weis, Temporal evolution of the Kerguelen plume: Geochemical evidence from ~38 to 82 Ma lavas forming the Ninetyeast Ridge, Contrib. Mineral. Petrol. 121 (1995) 12–28.
[22] D. Weis, F.A. Frey, Isotope geochemistry of Ninetyeast Ridge basement basalts: Sr, Nd, and Pb evidence for involvement of the Kerguelen Hotspot, in: J. Weissel, J. Peirce, E. Taylor, J. Alt et al. (Eds.), Proc. ODP, Sci. Results, 121, Ocean Drilling Program, College Station, TX, 1991, pp. 591–610.
[23] K.H. Rubin, J.D. Macdougall, M.R. Perfit, ^{210}Po–^{210}Pb dating of recent volcanic eruptions on the sea floor, Nature 368 (1994) 841–844.
[24] K.H. Rubin, J.D. Macdougall, Submarine magma degassing and explosive magmatism at Macdonald (Tamarii) seamount, Nature 341 (1989) 50–52.
[25] A.H.F. Robertson, Cyprus umbers: Basalt–sediment relationships on a Mesozoic oceanic ridge, J. Geol. Soc. Lond. 131 (1975) 511–531.
[26] A.H.F. Robertson, Origins of ochres and umbers: Evidence from Skouriotissa, Troodos Massif, Cyprus, Trans. Inst. Min. Metall. Sect. B 85 (1976) B245–B251.
[27] R.A. Mills, T. Clayton, J.C. Alt, Low-temperature fluid flow through sulfidic sediments from TAG: Modification of fluid chemistry and alteration of mineral deposits, Geophys. Res. Lett. 23 (1996) 3495–3498.
[28] D.S. Scheirer, E.T. Baker, K.T.M. Johnson, Detection of hydrothermal plumes along the Southeast Indian Ridge near the Amsterdam–St. Paul Plateau, Geophys. Res. Lett. 25 (1) (1998) 97–100.
[29] E.T. Baker, H.T. Milburn, MAPR: a new instrument for hydrothermal plume mapping, RIDGE Events 8 (1997) 23–25.
[30] B.M. Gunn, S.E. Abranson, J. Nougier, N.D. Watkins, A. Hajash, Amsterdam Island, an isolated volcano in the southern Indian Ocean, Contrib. Mineral. Petrol. 32 (1971) 79–92.
[31] B.M. Gunn, N.D. Watkins, W.E. Trzcienski, J. Nougier, The Amsterdam–St. Paul volcanic province, and the formation of low Al tholeitic andesites, Lithos 8 (1975) 137–149.
[32] R. Hébert, Petrology of a South–East Indian Ridge segment between 28° and 41°S and the origin of St. Paul Island, Indian Ocean: I. Mineralogy and major and minor elements chemistry, Ofioliti 12 (1987) 357–391.
[33] J. Nougier, J.W. Thomson, Amsterdam and Saint Paul Islands, in: W.E. LeMasurier, J.W. Thomson, P.E. Baker, P.R. Kyle, P.D. Rowley, J.L. Smellie, W.J. Verwoerd (Eds.), Volcanoes of the Antarctic Plate and Southern Oceans, Antarctic Research Series 48, American Geophysical Union, Washington, DC, 1990, pp. 442–445.
[34] R.A. Mills, H. Elderfield, Rare earth element geochemistry of hydrothermal deposits from the active TAG Mound, 26°N Mid-Atlantic Ridge, Geochim. Cosmochim. Acta 59 (1995) 3511–3524.
[35] M.K. Tivey, S.E. Humphris, G. Thompson, M.D. Hannington, P.A. Rona, Deducing patterns of fluid flow and mixing within the TAG active hydrothermal mound using mineralogical and geochemical data, J. Geophys. Res. 100 (1995) 12527–12555.
[36] K.H. Rubin, Degassing of metals and metalloids from erupting seamount and mid-ocean ridge volcanoes: Observations and predictions, Geochim. Cosmochim. Acta 61 (1997) 3525–3542.
[37] E.T. Baker, A. Tennant, R.A. Feely, G.T. Lebon, S.L. Walker, Field and laboratory studies on the effect of particle size and composition on optical backscattering measurements in hydrothermal plumes, Deep-Sea Res. (2000), in press.
[38] J.S. Turner, Buoyancy Effects in Fluids, Chapter 8, Cambridge Univ. Press, Cambridge, 1973.
[39] M. Kusakabe, G.Z. Tanyileke, S.A. McCord, Recent pH and CO_2 profiles at Lakes Nyos and Monoun, Cameroon: Implications for the degassing strategy and its numerical simulation, J. Volcanol. Geotherm. Res. (2000), in press.
[40] D.A. Ross, Temperature structure of Red Sea brines, in: E.T. Degens, D.A. Ross (Eds.), Hot Brines and Recent Heavy Metal Deposits in the Red Sea, Springer-Verlag, New York, 1969, pp. 148–152.
[41] M. Girod, G. Camus, Y. Vialette, Sur la présence de tholéiites à l'île Saint-Paul (Océan Indien), Contrib. Mineral. Petrol. 33 (1971) 108–117.
[42] E. Anders, N. Grevesse, Abundances of the elements: meteoritic and solar, Geochim. Cosmochim. Acta 53 (1989) 197–214.
[43] D. Weis, F.A. Frey, H. Leyrit, I. Gautier, Kerguelen Archipelago revisited: geochemical and isotopic study of the southeast province lavas, Earth Planet. Sci. Lett. 118 (1993) 101–119.
[44] W.M. White, A.W. Hofmann, Sr and Nd isotope geochemistry of oceanic basalts and mantle evolution, Nature 296 (1982) 821–825.
[45] D. Weis, J.-F. Beaux, I. Gautier, A. Giret, P. Vidal, Kerguelen archipelago: geochemical evidence for recycled ma-

terial, in: S.R.H.a.L. Gülen (Ed.), Crust/Mantle Recycling at Convergence Zones, NATO ASI Series, Kluwer Academic Press, Amsterdam, 1989, pp. 59–63.

[46] D. Weis, Y. Bassias, I. Gautier, J.-P. Mennessier, Dupal anomaly in existence 115 Ma ago: evidence from isotopic study of the Kerguelen Plateau (South Indian Ocean), Geochim. Cosmochim. Acta 53 (1989) 2125–2131.

[47] H.-J. Yang, F.A. Frey, D. Weis, A. Giret, D. Pyle, G. Michon, Petrogenesis of the flood basalts forming the northern Kerguelen Archipelago: Implications for the Kerguelen Plume, J. Petrol. 39 (1998) 711–748.

[48] D. Weis, F.A. Frey, A. Giret, J.-M. Cantagrel, Geochemical characteristics of the youngest volcano (Mount Ross) in the Kerguelen Archipelago: Inferences for magma flux, lithosphere assimilation and composition of the Kerguelen Plume, J. Petrol. 39 (1998) 973–994.

[49] D. Weis, F.A. Frey, Role of Kerguelen Plume in generating the eastern Indian Ocean seafloor, J. Geophys. Res. 101 (1996) 13831–13849.